



# Abiotic redox reactions in hydrothermal mixing zones: Decreased energy availability for the subsurface biosphere

Jill M. McDermott<sup>a,1,2</sup>, Sean P. Sylva<sup>a</sup>, Shuhei Ono<sup>b</sup>, Christopher R. German<sup>c</sup> , and Jeffrey S. Seewald<sup>a</sup>

<sup>a</sup>Department of Marine Chemistry and Geochemistry, Woods Hole Oceanographic Institution, Woods Hole, MA 02543; <sup>b</sup>Department of Earth, Atmospheric and Planetary Sciences, Massachusetts Institute of Technology, Cambridge, MA 02139; and <sup>c</sup>Department of Geology and Geophysics, Woods Hole Oceanographic Institution, Woods Hole, MA 02543

Edited by Donald E. Canfield, Institute of Biology and Nordic Center for Earth Evolution, University of Southern Denmark, Odense M., Denmark, and approved July 14, 2020 (received for review February 18, 2020)

**Subseafloor mixing of high-temperature hot-spring fluids with cold seawater creates intermediate-temperature diffuse fluids that are replete with potential chemical energy. This energy can be harnessed by a chemosynthetic biosphere that permeates hydrothermal regions on Earth. Shifts in the abundance of redox-reactive species in diffuse fluids are often interpreted to reflect the direct influence of subseafloor microbial activity on fluid geochemical budgets. Here, we examine hydrothermal fluids venting at 44 to 149 °C at the Piccard hydrothermal field that span the canonical 122 °C limit to life, and thus provide a rare opportunity to study the transition between habitable and uninhabitable environments. In contrast with previous studies, we show that hydrocarbons are contributed by biomass pyrolysis, while abiotic sulfate (SO<sub>4</sub><sup>2-</sup>) reduction produces large depletions in H<sub>2</sub>. The latter process consumes energy that could otherwise support key metabolic strategies employed by the subseafloor biosphere. Available Gibbs free energy is reduced by 71 to 86% across the habitable temperature range for both hydrogenotrophic SO<sub>4</sub><sup>2-</sup> reduction to hydrogen sulfide (H<sub>2</sub>S) and carbon dioxide (CO<sub>2</sub>) reduction to methane (CH<sub>4</sub>). The abiotic H<sub>2</sub> sink we identify has implications for the productivity of subseafloor microbial ecosystems and is an important process to consider within models of H<sub>2</sub> production and consumption in young oceanic crust.**

hydrothermal vent | subsurface biosphere | bioenergetics | biogeochemistry

At deep-sea hydrothermal vents, fluid–mineral reactions taking place at high temperatures and pressures substantially influence the chemical composition of the world’s oceans (1, 2) and sustain thriving microbiological communities below and at the seafloor (3–6). Mixing between hot, chemically reduced hydrothermal fluids and cold, oxidized seawater in the subsurface creates moderate-temperature diffuse vent fluids and large amounts of potential chemical energy. Chemosynthetic microbes harness this chemical energy by catalyzing thermodynamically favorable redox reactions that support the primary fixation of inorganic CO<sub>2</sub> into biomass (5, 7, 8).

Numerous field investigations have demonstrated that vent fluid temperature and composition can control variability in modern-day microbial community structure and function (3–6) and provide insight into the environmental driving forces of evolution (9, 10). The close linkage between vent microbiology and fluid chemistry is further supported by thermodynamic models that estimate available energy for specific metabolic reactions (7, 11–13). Beyond serving as the primary producers at the base of the food web in hydrothermal environments, microbial activity has important biogeochemical implications, as metabolic processes can modulate the composition of diffuse fluids via the consumption and production of redox-reactive species within mixtures of endmember hydrothermal source fluids and seawater (14–23).

In addition to modification by active microbial processes, abiotic reactions and thermogenic reactions that involve thermal decomposition of living or once-living biomass can also exert important controls on diffuse fluid chemistry and microbial ecosystems. In particular, abiotic redox reactions that proceed rapidly and consume reactants utilized by microorganisms will reduce available metabolic energy, while thermogenic production of hydrocarbons represents a source of carbon and energy that can support a heterotrophic lifestyle.

Here, we report on the composition of low-temperature vent fluids (44 to 149 °C) sampled in 2012 and 2013 at the Piccard hydrothermal field, Mid-Cayman Rise (Tables 1 and 2, and *SI Appendix*, Tables S1 and S2). Hosted in unconsolidated pillow basalts and sheet flows at a water depth of 4,970 m along the eastern flank of an ultraslow spreading (15 to 17 mm/y full rate), 12-km-long axial volcanic ridge, Piccard is Earth’s deepest known vent field (24). Low-temperature fluid compositions indicate that they are formed by subseafloor mixing of cold (5 °C) seawater and 398 °C vent fluids represented by the nearby Beebe Vents black smokers. These high-temperature vents share a common major ion and dissolved volatile chemistry that reflects a single vapor phase, low-Cl source fluid that originates at temperatures

## Significance

**Hydrothermal fluid geochemistry exerts a key control on subseafloor microbial community structure and function. However, the effects of microbial metabolic activity, thermal decomposition of biomass, and abiotic reactions on geochemistry remain unconstrained. Depletions in molecular hydrogen and enrichments in methane in submarine hydrothermal mixing zones have been interpreted to reflect the influence of an active subseafloor biosphere. In contrast, our work reveals that these chemical shifts are driven by abiotic and thermogenic processes at temperatures beyond the limit for life. These findings have critical implications for constraining the extent to which global geochemical cycles can sustain a deep biosphere, and for the global molecular hydrogen budget.**

Author contributions: C.R.G. and J.S.S. designed research; J.M.M., S.P.S., S.O., C.R.G., and J.S.S. performed research; J.M.M. and S.P.S. contributed new reagents/analytic tools; J.M.M., C.R.G., and J.S.S. analyzed data; and J.M.M., C.R.G., and J.S.S. wrote the paper.

The authors declare no competing interest.

This article is a PNAS Direct Submission.

This open access article is distributed under [Creative Commons Attribution-NonCommercial-NoDerivatives License 4.0 \(CC BY-NC-ND\)](https://creativecommons.org/licenses/by-nc-nd/4.0/).

<sup>1</sup>Present address: Department of Earth and Environmental Sciences, Lehigh University, Bethlehem, PA 18015.

<sup>2</sup>To whom correspondence may be addressed. Email: [jillmcdermott@alum.mit.edu](mailto:jillmcdermott@alum.mit.edu).

This article contains supporting information online at <https://www.pnas.org/lookup/suppl/doi:10.1073/pnas.2003108117/-DCSupplemental>.

First published August 12, 2020.

**Table 1. Measured aqueous species abundances in mixing zones at the Piccard vent field**

Vent (year)/sample*	$T_{max}$ , °C	Mg, mm	pH, 25 °C	Ca, mm	SO <sub>4</sub> , mm	Fe, mm	ΣHCOOH, μm
Beebe endmember <sup>†</sup>		0	— <sup>‡</sup>	6.18	0.21	6.58	—
Hot Chimlet 1 (2012)							
J2-619-IGT6	149	35.4	5.1	7.15	15.2	0.85	54
J2-619-IGT3	147	33.4	5.0	6.93	13.8	— <sup>§</sup>	58
Hot Chimlet 1 (2013)							
N59-IGT6	81	41.5	5.8	10.4	20.7	0.50	13
N59-IGT4	85	50.4	6.3	10.3	26.4	0.17	<1.0
Hot Chimlet 3 (2013)							
N62-IGT8	101	47.1	6.0	10.3	24.7	— <sup>§</sup>	55
N62-IGT7	97	35.1	5.4	10.2	16.6	0.35	167
Hot Chimlet 2 (2012)							
J2-620-IGT4	95	45.4	5.7	9.35	24.2	0.15	16
J2-620-IGT8	87	47.8	5.9	9.75	23.1	0.16	12
Shrimp Gulley 1 (2012)							
J2-620-IGT1	111	42.4	5.5	9.67	22.6	1.89	24
J2-620-IGT2	104	44.8	5.6	10.1	22.8	1.58	18
Shrimp Gulley 3 (2013)							
N63-IGT6	80	47.9	5.8	10.1	24.6	2.56	<1.0
Shrimp Gulley 2 (2012)							
J2-618-IGT1	45	47.4	6.0	10.2	25.4	0.091	9.4
J2-618-IGT3	44	48.9	5.9	10.1	25.2	0.11	8.8
Bottom seawater	~5	52.5	8.0	10.3	28.0	0.0	<1.0

\*Jason (J2) or Nereus (N##) dive number and isobaric gas-tight sampler number (-IGT).

<sup>†</sup>Average high-temperature vent endmember [for Beebe 1, 3, 5, and Beebe Woods; McDermott et al. (25)]. See McDermott et al. (25) for IGT data from high-temperature fluid samples.

<sup>‡</sup>Lowest measured pH for high-temperature source fluids: 3.1 (Beebe Vent 1, 2012); 3.2 (Beebe Vent 3, 2012); 3.0 (Beebe Vent 5, 2012); 3.2 (Beebe Vent 5, 2013); 3.2 (Beebe Woods, 2012); from McDermott et al. (25).

<sup>§</sup>A dregs aliquot was not collected for sample J2-619-IGT3 or N62-IGT8. The dregs aliquot is composed of particles remaining in the IGT sampler following extraction of the aqueous sample; see *Methods and Materials*.

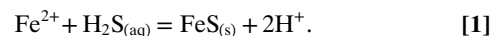
that potentially exceed 500 °C due to the great depth of the system (25). Many of the low-temperature Piccard fluids were turbid at the time of venting, suggesting that they contain fine-grained particulate material. The high-temperature Beebe Vents are characterized by dissolved H<sub>2</sub> concentrations as high as 20.7 mmol/L due to high temperatures in subsurface reaction zones (25), making the lower temperature diffuse fluids at Piccard ideally suited to assess processes that may consume H<sub>2</sub> and the abundance of other redox-reactive species in near seafloor mixing zones. The fate of H<sub>2</sub> generated in young oceanic crust is of high interest, as a recent synthesis study cannot account for at least 30% of all H<sub>2</sub> produced (26). Although uptake by subsurface microbial metabolic activity is inferred to be the primary driver for these H<sub>2</sub> losses, it is critically important to consider the possibility of abiotic sinks for H<sub>2</sub>. An abiotic H<sub>2</sub> sink could vastly affect global H<sub>2</sub> budgets and estimates of subsurface biosphere productivity.

### Abiotic Processes in Subseafloor Mixing Environments

Because dissolved Mg<sup>2+</sup> behaves conservatively during mixing of near-zero-Mg endmember high-temperature vent fluids and Mg-rich seawater, the effects of subseafloor mixing on a given aqueous species in a mixed vent fluid can be examined by plotting its concentration against Mg<sup>2+</sup> (Fig. 1). Many species such as Cl<sup>-</sup> show conservative behavior during mixing in the Piccard fluids (Fig. 1A), demonstrating their origin from simple two-component subsurface mixing between seawater and Beebe Vents fluids. However, several redox-reactive species behave nonconservatively and show significant depletions or enrichments (Fig. 1 and *SI Appendix, Table S3*). For example, concentrations of dissolved H<sub>2</sub>, ΣH<sub>2</sub>S (ΣH<sub>2</sub>S = H<sub>2</sub>S + HS<sup>-</sup> + S<sup>2-</sup>), and SO<sub>4</sub><sup>2-</sup> show substantial depletions (Fig. 1B–D), while dissolved ΣHCOOH (ΣHCOOH = HCOO<sup>-</sup> + HCOOH) and hydrocarbons show varying levels of enrichment (Fig. 1E–I).

Dissolved Ca<sup>2+</sup> and Fe<sup>2+</sup> concentrations show both enrichments and depletions relative to conservative mixing (Fig. 1J and K). In the case of Fe<sup>2+</sup>, enriched concentrations may reflect entrainment of Fe-rich particles during sample collection (27). Some of the most pronounced depletions and enrichments are observed in the Hot Chimlet 1 fluids sampled in 2012. This fluid is characterized by a maximum measured temperature of 149 °C that exceeds the known temperature limit for life at 122 °C (28). Accordingly, we infer that consumption of H<sub>2</sub>, the production of CH<sub>4</sub>, and the nonconservative behavior of many other species at Hot Chimlet 1 (2012) must proceed via one or more abiotic processes.

Removal of dissolved ΣH<sub>2</sub>S and Fe<sup>2+</sup> from mixed fluids can be attributed to the precipitation of iron sulfide minerals due to decreases in their solubility with decreasing temperature and increasing pH. Near equimolar depletions of ΣH<sub>2</sub>S and Fe<sup>2+</sup> that range from 0.88 to 1.85 mmol/kg in the Hot Chimlet 1 fluids in both 2012 and 2013 and the Hot Chimlet 3 fluids (*SI Appendix, Table S3*) suggest pyrrhotite (FeS) formation during mixing according to the following reaction:



Phase relations in the chemical system Fe–S–O–H indicate that pyrrhotite is the stable iron phase for the measured concentrations of ΣH<sub>2</sub>S and H<sub>2</sub> in the endmember fluids to temperatures down to 150 °C (Fig. 2), consistent with pyrrhotite formation during the early stages of vent fluid mixing with cold seawater. Continued seawater mixing produces temperatures below 150 °C and reduces dissolved H<sub>2</sub> concentrations, shifting fluid compositions into the pyrite (FeS<sub>2</sub>) stability field (Fig. 2). Accordingly, pyrite formation may be responsible for additional depletion in ΣH<sub>2</sub>S and Fe<sup>2+</sup> during the later stages of mixing under temperature conditions compatible with life.

**Table 2. Measured volatile species abundances and isotope values in mixing zones at the Piccard vent field**

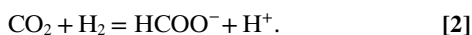
Vent (year)/ sample*	$\Sigma\text{H}_2\text{S}$ , mm	$\delta^{34}\text{S}_{\text{H}_2\text{S}}$ , ‰	$\text{H}_2$ , mm	$\Sigma\text{CO}_2$ , mm	$\text{CH}_4$ , $\mu\text{m}$	$\text{C}_2\text{H}_6$ , nm	$\text{C}_3\text{H}_8$ , nm	n-C <sub>4</sub> H <sub>10</sub> , nm	i-C <sub>4</sub> H <sub>10</sub> , nm	$\delta^{13}\text{C}_{\text{CH}_4}$ , ‰	$\delta^{13}\text{C}_{\text{C}_2\text{H}_6}$ , ‰	$\delta^{13}\text{C}_{\text{C}_3\text{H}_8}$ , ‰
Beebe endmember <sup>†</sup>	11.7	6.1	19.4	25.7	121	13	7.6	1.9	1.3	-23.9	-24.9	-
Hot Chimlet 1 (2012)												
J2-619-IGT6	2.47	6.6	1.94	9.09	51.2	43	28	9.0	9.7	-28.4	-33.3	-29.7
J2-619-IGT3	2.60	—	2.06	10.1	56.5	92	66	27	11	-29.9	-33.5	-28.2
Hot Chimlet 1 (2013)												
N59-IGT6	1.47	—	0.027	—	39.6	27	22	5.4	5.2	—	—	—
N59-IGT4	0.086	—	0.010	—	9.78	—	—	—	—	—	—	—
Hot Chimlet 3 (2013)												
N62-IGT8	0.45	—	0.13	—	23.0	—	—	—	—	—	—	—
N62-IGT7	2.03	—	0.45	—	64.3	36	28	7.3	7.7	—	-36.9	-29.5
Hot Chimlet 2 (2012)												
J2-620-IGT4	1.04	—	0.68	4.89	21.8	17	11	4.3	3.4	-29.2	—	—
J2-620-IGT8	0.96	—	0.52	4.08	15.6	11	8.3	3.1	<1.0	—	—	—
Shrimp Gulley 1 (2012)												
J2-620-IGT1	1.95	—	0.40	5.95	24.0	14	9.7	3.8	1.6	—	—	—
J2-620-IGT2	1.12	—	0.28	5.56	20.5	12	7.3	2.7	<1.0	—	—	—
Shrimp Gulley 3 (2013)												
N63-IGT6	0.49	—	<0.002	—	19.4	—	—	—	—	—	—	—
Shrimp Gulley 2 (2012)												
J2-618-IGT1	0.83	—	0.11	3.39	10.8	5.1	—	1.6	<1.0	—	—	—
J2-618-IGT3	0.84	—	0.13	3.64	10.9	5.1	4.0	1.8	<1.0	—	—	—
Bottom seawater	0	—	0	2.21	0	0	0	0.0	0	—	—	—

\*Jason (J2) or Nereus (N##) dive number and isobaric gas-tight sampler number (-IGT).

<sup>†</sup>Average high-temperature vent endmember [for Beebe 1, 3, 5, and Beebe Woods; McDermott et al. (25)]. See McDermott et al. (25) for IGT data from high-temperature fluid samples.

The formation of iron sulfides such as pyrrhotite according to reaction 1 results in the generation of 2 equivalents of acidity for each mole of  $\Sigma\text{H}_2\text{S}$  and  $\text{Fe}^{2+}$  that precipitates. Thus, the Hot Chimlet 3 fluids that display the largest  $\Sigma\text{H}_2\text{S}$  and  $\text{Fe}^{2+}$  depletion of 1.85 mmol/kg will generate acidity at a level sufficient to titrate all of the alkalinity contributed by admixed seawater and create fluids characterized by pH (25 °C) <3 in the absence of other reactions that consume  $\text{H}^+$ . Measured pH (25 °C) values for all of the mixed fluids are >5, providing evidence for titration of acidity by additional geochemical processes.

Enrichment of the mixed Piccard fluids in  $\Sigma\text{HCOOH}$  suggests that  $\text{CO}_2$  reduction during mixing may account for a portion of the observed  $\text{H}_2$  depletions. Reducing conditions, coupled with the lower temperatures and higher pH conditions of a mixed fluid, provide a thermodynamic drive for the abiotic reduction of  $\text{CO}_2$  by  $\text{H}_2$  to  $\Sigma\text{HCOOH}$  according to the following reaction:



Calculated chemical affinities for reaction 2 in >100 °C mixed fluids are less than  $\pm 5$  kJ/mol, suggesting that they have attained metastable thermodynamic equilibrium between  $\text{CO}_2$ ,  $\text{H}_2$ , and  $\Sigma\text{HCOOH}$ . Calculated affinities in the <100 °C fluids are slightly higher than those at >100 °C with positive values of +8.6 kJ/mol, suggesting a thermodynamic drive for additional  $\Sigma\text{HCOOH}$  production that may reflect slower reaction kinetics at lower temperatures of these fluids. A similar approach to equilibrium involving  $\text{CO}_2$ ,  $\text{H}_2$ , and  $\Sigma\text{HCOOH}$  has been documented at the nearby Von

Damm vent field (29) and at the Lost City vent field, Mid-Atlantic Ridge (30). Attainment of metastable equilibrium according to reaction 2 in subsurface mixing zones represents an abiotic pathway for the production of  $\Sigma\text{HCOOH}$  that may fuel microbial metabolism (6).

Although formation of  $\Sigma\text{HCOOH}$  in subsurface mixing zones consumes  $\text{H}_2$  according to reaction 2, the relatively low concentrations observed indicate that it can account for only a small fraction of the  $\text{H}_2$  depletions in the mixed fluids. For example, close examination of the 149 °C Hot Chimlet 1 fluid in 2012 (J2-619-IGT6, Tables 1 and 2) reveals a  $\text{H}_2$  depletion of 4.3 mmol/kg (Fig. 1B) that was accompanied by production of only 0.052 mmol/kg  $\Sigma\text{HCOOH}$  (Fig. 1E). Relatively minor depletions in  $\Sigma\text{CO}_2$  (Fig. 1L;  $\Sigma\text{CO}_2 = \text{H}_2\text{CO}_3^* + \text{HCO}_3^- + \text{CO}_3^{2-}$ ) indicate that reduction of  $\Sigma\text{CO}_2$  to other reduced carbon species is not responsible for the large  $\text{H}_2$  depletions in the mixed fluids. Rather, the linear relationship between  $\Sigma\text{CO}_2$  and Mg abundances (Fig. 1L) largely reflects mixing of a high  $\Sigma\text{CO}_2$  endmember with lower  $\Sigma\text{CO}_2$  seawater. Minor amounts of  $\text{H}_2$  may also be consumed by reaction with dissolved  $\text{O}_2$  and  $\text{NO}_3^-$  present in admixed seawater at concentrations of  $\sim 0.2$  and  $\sim 0.02$  mmol/kg, respectively (31). Collectively,  $\Sigma\text{HCOOH}$  production and  $\text{O}_2$  and  $\text{NO}_3^-$  reduction can consume  $\sim 0.4$  mmol/kg of  $\text{H}_2$  in the 2012 Hot Chimlet 1 fluid, requiring an additional sink for the remaining 3.9 mmol/kg of  $\text{H}_2$  depletion.

High concentrations of dissolved  $\text{SO}_4^{2-}$  in conjunction with depletions relative to conservative values in mixed fluids suggest that reactions involving the reduction of  $\text{SO}_4^{2-}$  are responsible

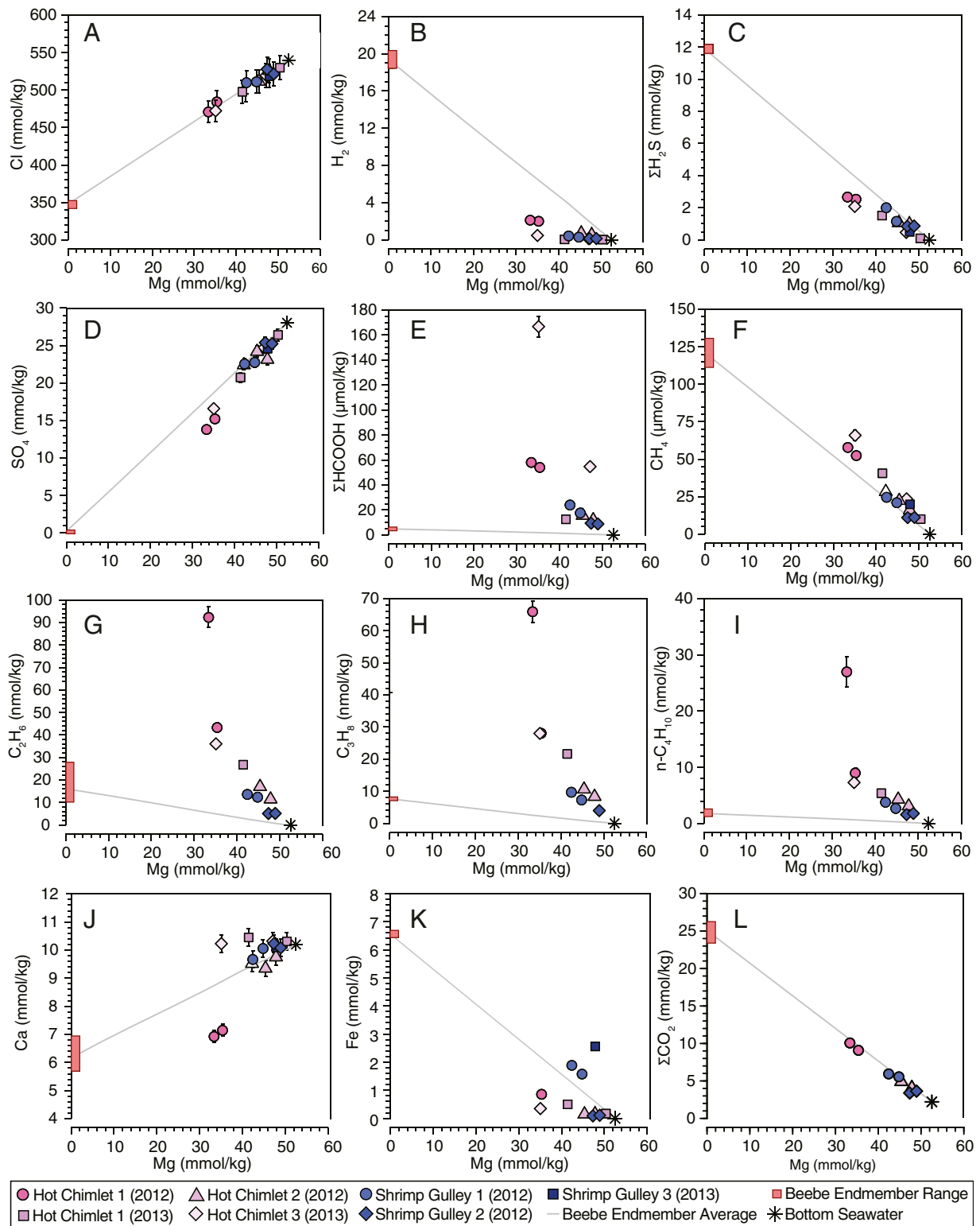


**Fig. 1.** Measured concentrations of aqueous Mg versus aqueous Cl (A), H<sub>2</sub> (B), ΣH<sub>2</sub>S (C), SO<sub>4</sub> (D), ΣHCOOH (E), CH<sub>4</sub> (F), C<sub>2</sub>H<sub>6</sub> (G), C<sub>3</sub>H<sub>8</sub> (H), n-C<sub>4</sub>H<sub>10</sub> (I), Ca (J), Fe (K), and ΣCO<sub>2</sub> (L) for mixed fluids sampled at the Piccard vent field in 2012 and 2013. For each species, the range in extrapolated zero-Mg high-temperature endmember composition is shown with the red bar along the y axis, and the average is shown with a gray line projected from seawater composition. Species that exhibit conservative behavior during mixing plot on the line, while species that behave nonconservatively plot above or below the line. The 2σ errors are shown (or are smaller than the symbols).

for the observed H<sub>2</sub> depletions. Complete SO<sub>4</sub><sup>2-</sup> reduction results in the production of ΣH<sub>2</sub>S, while partial reduction may form sulfur species in intermediate states such as sulfur (S), thiosulfate

(S<sub>2</sub>O<sub>3</sub><sup>2-</sup>), or polysulfide (S<sub>x</sub><sup>2-</sup>). Equilibrium fractionation factors for isotopic exchange between SO<sub>4</sub><sup>2-</sup> and ΣH<sub>2</sub>S (32) indicate that reduction of SO<sub>4</sub><sup>2-</sup> at temperatures below 400 °C should produce

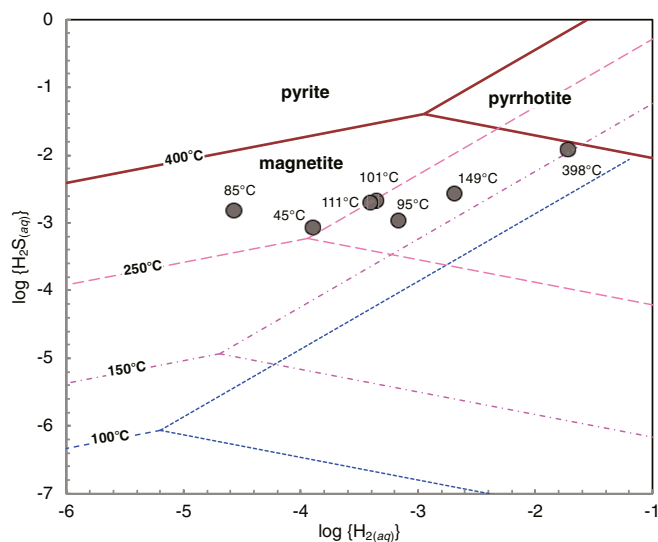
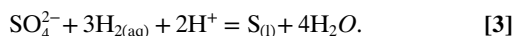


**Fig. 2.** Activity diagram showing phase relations in the chemical system Fe–S–O–H at 400, 250, 150, and 100 °C and 500 bar. The symbols indicate measured  $\text{H}_2(\text{aq})$  and  $\text{H}_2\text{S}(\text{aq})$  concentrations in Piccard vent fluids. Requisite thermodynamic data for the construction of the diagram were calculated using SUPCRT92 computer code (56) and corrected for the nonstoichiometric composition of pyrrhotite in equilibrium with pyrite (57).

$\Sigma\text{H}_2\text{S}$  that is highly depleted in  $^{34}\text{S}$  relative to initial seawater  $\text{SO}_4^{2-}$  ( $\delta^{34}\text{S}_{\text{seawater SO}_4} = 21.0\text{‰}$ ). For example,  $\Sigma\text{H}_2\text{S}$  produced from seawater  $\text{SO}_4^{2-}$  at 350 °C would have a  $\delta^{34}\text{S}$  value of 4.1‰ at 350 °C and  $-2.5\text{‰}$  at 250 °C (32), resulting in decreasing  $\delta^{34}\text{S}$  values for dissolved  $\Sigma\text{H}_2\text{S}$  in low-temperature mixed fluids. Comparison of the  $^{34}\text{S}$  content of  $\Sigma\text{H}_2\text{S}$  in the high-temperature endmember fluid with the  $^{34}\text{S}$  content of  $\Sigma\text{H}_2\text{S}$  in the 2012 Hot Chimlet 1 fluid reveals near-identical values of 6.1 and 6.6‰, respectively, indicating that significant amounts of  $\Sigma\text{H}_2\text{S}$  produced by  $\text{SO}_4^{2-}$  reduction during mixing have not been added to the low-temperature fluids. The absence of evidence for reduction of  $\text{SO}_4^{2-}$  to  $\Sigma\text{H}_2\text{S}$  suggests that the observed  $\text{H}_2$  depletions reflect formation of intermediate oxidation state sulfur species.

The formation of intermediate oxidation state sulfur species has been reported for several low-temperature vent environments (18, 33, 34) but was not determined in this study. We postulate that the  $\text{H}_2$  depletions observed in the low-temperature Piccard fluids result from the formation of elemental S,  $\text{S}_2\text{O}_3^{2-}$ , and  $\text{S}_x^{2-}$  (Fig. 3). Indeed, the distinct turbidity that characterized many of the low-temperature Piccard fluids may reflect condensation of liquid or particulate sulfur. Reduction of seawater  $\text{SO}_4^{2-}$  to an intermediate oxidation state such as elemental S can be represented by the following reaction:



Reaction 3 predicts that each mole of  $\text{SO}_4^{2-}$  reduced will consume 3 mol of  $\text{H}_2$  and 2 mol of  $\text{H}^+$ , indicating that formation of elemental S may represent a sink for acidity produced by precipitation of iron sulfides according to reaction 1 in addition to dissolved  $\text{H}_2$ . The 3.9 mmol/kg  $\text{H}_2$  depletion in the 2012 Hot Chimlet 1 fluid that cannot be attributed to reduction of  $\Sigma\text{CO}_2$ ,  $\text{O}_2$ , and  $\text{NO}_3^-$  would be consistent with the reduction of 1.3 mmol/kg  $\text{SO}_4^{2-}$ . The observed  $\text{SO}_4^{2-}$  depletion of 3.7 mmol/kg in this fluid (Fig. 1D and *SI Appendix, Table S3*) is substantially greater than this value, but includes removal of  $\text{SO}_4^{2-}$  due to anhydrite ( $\text{CaSO}_4$ ) precipitation. Due to significant variability in the endmember fluid Ca concentration (Fig. 1K), estimates for the amount of anhydrite precipitation based on Ca

depletions vary from 1.6 to 2.3 mmol/kg, suggesting that 1.4 to 2.1 mmol/kg of the  $\text{SO}_4^{2-}$  depletion can be attributed to formation of intermediate oxidation state sulfur species. Although the low end of this range is consistent with the observed  $\text{H}_2$  depletion via elemental S formation (reaction 3), the higher values may suggest production of more oxidized intermediate oxidation state sulfur species, such as  $\text{S}_2\text{O}_3^{2-}$ , that would consume less  $\text{H}_2$  for a given amount of  $\text{SO}_4^{2-}$  reduced.

In contrast to the Hot Chimlet 1 (2012) fluid, measured temperatures of all other mixing zone fluids collected in 2012 and 2013 are below the canonical 122 °C limit for life. Thus, the chemistry of these fluids could be impacted by active microbial processes in addition to abiotic processes (Fig. 3). It is important to note, however, that this 122 °C record is held by a methanogen grown in the laboratory under optimal conditions (28). In the natural environment, the limit for life may be closer to 80 °C, as has been shown in petroleum basin systems (35). Eleven of 13 fluids in this study match or exceed 80 °C, and thus the chemistry of the majority of our samples may reflect only abiotic or thermogenic inputs. All fluids have lost significant quantities of  $\text{H}_2$  relative to conservative mixing calculations (0.77 to 5.98 mmol/kg  $\text{H}_2$  lost; Fig. 1B and *SI Appendix, Table S3*). Common metabolic reactions that directly impact  $\text{H}_2$ , such as aerobic  $\text{H}_2$  oxidation, can be eliminated as significant, due to insufficient  $\text{O}_2$  availability to account for the magnitude of  $\text{H}_2$  lost.

Mixed fluids sampled in 2013 at Hot Chimlet 1, Hot Chimlet 3, and Shrimp Gulley 3 have temperatures of 80, 101, and 85 °C, respectively, and are characterized by significant  $\text{SO}_4^{2-}$  depletions from 0.5 to 2.2 mmol/kg (Fig. 1D and *SI Appendix, Table S3*). These  $\text{SO}_4^{2-}$  depletions are accompanied by  $\text{Ca}^{2+}$  enrichments relative to conservative mixing (Fig. 1J and *SI Appendix, Table S3*) indicating net dissolution of anhydrite, which would have contributed additional  $\text{SO}_4^{2-}$  to the fluid in 1:1 proportion to  $\text{Ca}^{2+}$ . The observation that  $\text{SO}_4^{2-}$  has been consumed in these fluids despite an additional source from dissolving anhydrite, highlights the importance of abiotic or microbially mediated  $\text{SO}_4^{2-}$  reduction pathways as a sink for  $\text{H}_2$ .

### Thermogenic Processes

In contrast to the depletions observed for inorganic redox reactive species, measured concentrations of  $\text{CH}_4$ ,  $\text{C}_2\text{H}_6$ ,  $\text{C}_3\text{H}_8$ ,  $n\text{-C}_4\text{H}_{10}$ , and  $i\text{-C}_4\text{H}_{10}$  in the low-temperature mixed fluids at the Piccard vent field are significantly greater than abundances expected for conservative mixing of endmember fluids and seawater, especially within the 149 °C Hot Chimlet fluid in 2012 (Table 2 and Fig. 1F–I). Several lines of evidence suggest that these hydrocarbon enrichments are the product of thermal degradation of immature organic material. Relative to biogenic and abiotic mantle-derived hydrocarbons that are dominated by  $\text{CH}_4$ , thermogenic hydrocarbons generally contain substantially greater proportions of  $\text{C}_{2+}$  alkanes (36). Thus, substantially lower  $\text{CH}_4/\text{C}_{2+}$  values (mol/mol) of 290 to 1,000 in the low-temperature mixed fluids relative to the high-temperature endmember fluids characterized by  $\text{CH}_4/\text{C}_{2+}$  values of 2,300 to 4,500, likely reflect a large increase in the relative abundance of thermogenic  $\text{C}_{2+}$  hydrocarbons. Similar processes have been noted in the high-temperature fluids at Piccard. For example, a higher  $\text{C}_2\text{H}_6$  concentration at Beebe Woods (354 °C, 28 nmol/kg) relative to the higher temperature Beebe Vents (398 °C, 11 to 15 nmol/kg) has been attributed to pyrolysis of dissolved organic carbon (DOC) in admixed seawater (25). Thermogenic hydrocarbon inputs are far more apparent in the mixed fluids presented here and represent a substantially greater fraction of the total hydrocarbon budgets. The linear inverse correlation of individual hydrocarbons with Mg in the diffuse fluids (Fig. 1) suggests that thermal alteration of organic matter occurs above the maximum temperature of 149 °C for the mixed fluids at

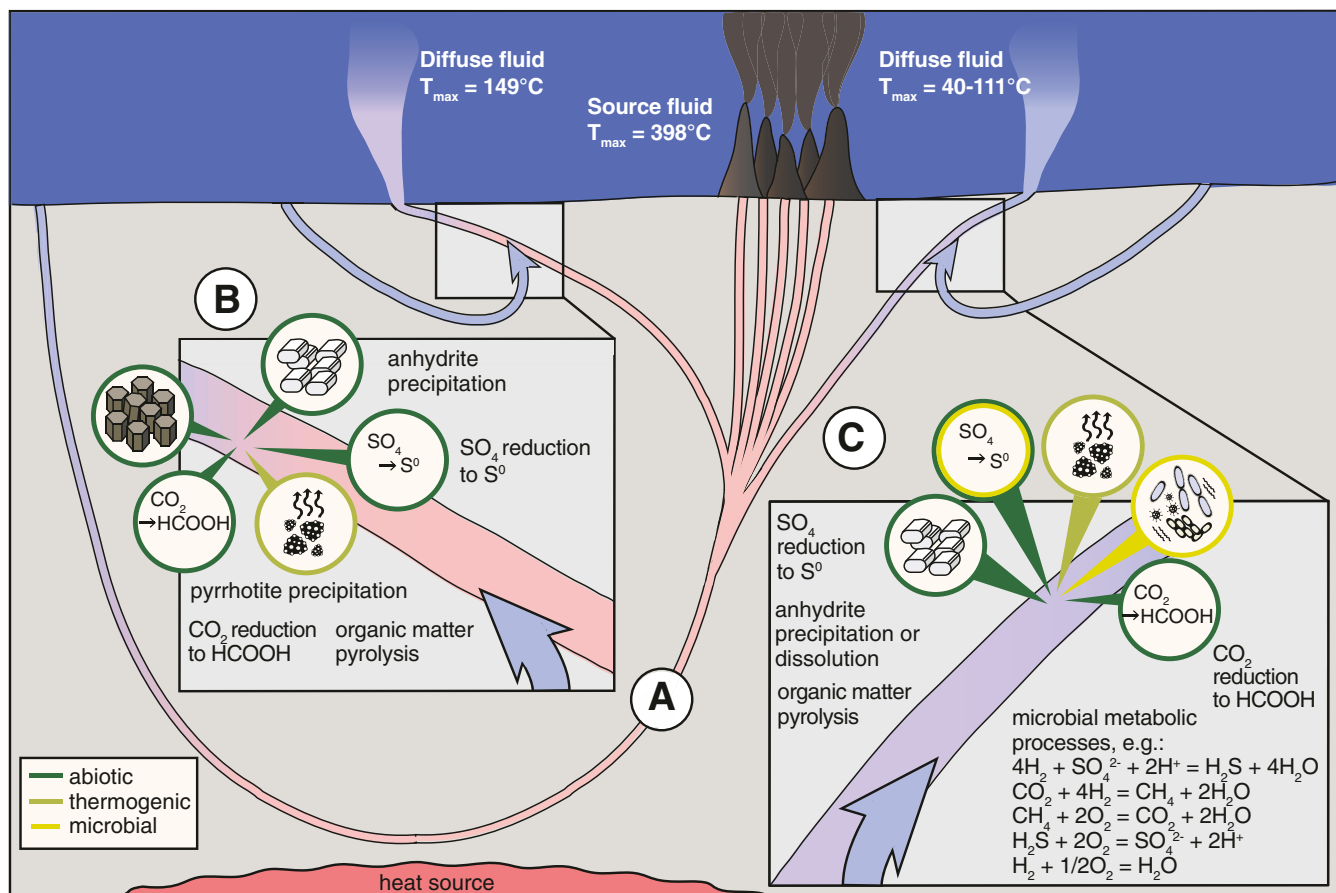


**Fig. 3.** Schematic representation of key processes that occur when ascending high-temperature source fluids mix with seawater (A) under relatively higher temperature ( $\sim 149^\circ\text{C}$ ) (B) and lower temperature ( $< 122^\circ\text{C}$ ) conditions (C). At temperatures of  $\sim 149^\circ\text{C}$  and higher, mixed fluid chemistry is impacted by abiotic reactions involving the aqueous reduction of dissolved species and mineral precipitation, along with thermogenic reactions involving the pyrolysis of living or previously living organic matter. At temperatures at and below  $122^\circ\text{C}$ , microbial metabolic processes may occur in addition to abiotic and thermogenic processes. The metabolic processes could include hydrogenotrophic  $\text{SO}_4^{2-}$  reduction, anaerobic methanogenesis from  $\text{CO}_2$  and  $\text{H}_2$ , methanotrophy by  $\text{O}_2$ , sulfide oxidation by  $\text{O}_2$ , and hydrogen oxidation by  $\text{O}_2$ .

Piccard, with subsequent seawater mixing producing decreasing hydrocarbon concentrations due to dilution.

The carbon isotopic composition of Hot Chimlet 1 hydrocarbons also supports a thermogenic origin for the hydrocarbon enrichment in the mixed fluids. The isotopic compositions of Hot Chimlet 1 hydrocarbons vary from  $-28.4$  to  $-29.9\text{‰}$  for  $\text{CH}_4$  and  $-33.3$  to  $-36.9\text{‰}$  for  $\text{C}_2\text{H}_6$  (Table 2). These values are significantly depleted in  $^{13}\text{C}$  relative to the  $^{13}\text{C}$  content of hydrocarbons in the endmember fluids that are characterized by uniform  $\delta^{13}\text{C}$  values of  $-23.9\text{‰}$  and  $-24.9\text{‰}$  for  $\text{CH}_4$  and  $\text{C}_2\text{H}_6$ , respectively. An isotope mass balance assuming two-component conservative mixing of hydrocarbons in endmember fluid (Table 2) with a thermogenic component added during mixing yields calculated  $\delta^{13}\text{C}$  values of  $-39.7$ ,  $-33.8$ , and  $-28.9\text{‰}$  for thermogenic  $\text{CH}_4$ ,  $\text{C}_2\text{H}_6$ , and  $\text{C}_3\text{H}_8$ , respectively. The calculated values fall within the range of  $-25\text{‰}$  to  $-50\text{‰}$  and show progressive  $^{13}\text{C}$  enrichment with increasing carbon chain length, consistent with trends typically observed for thermogenic hydrocarbons (37–39). The presence of hydrocarbons with similar isotopic compositions in mixed fluids with temperatures above and below  $122^\circ\text{C}$  suggests that they are derived from a common process occurring above and below the temperature limit for life (Fig. 3). The Piccard mixed fluids are also characterized by substantial enrichments in dissolved  $\Sigma\text{NH}_4$  ( $\Sigma\text{NH}_4 = \text{NH}_3 + \text{NH}_4^+$ ) and methanethiol ( $\text{CH}_3\text{SH}$ ) relative to the high-temperature endmembers (40) (SI Appendix, Table S1). Both species are

products of thermal degradation of fresh organic matter and provide additional evidence that thermogenic processes are contributing to the chemical inventory of mixed fluids at Piccard.

### Implications for Subsurface Life and Chemical Fluxes to the Ocean

Sulfate reduction rates and mechanisms have largely been studied within the context of petroleum reservoirs and sedimented basins, where  $\text{SO}_4^{2-}$  is reduced by organic matter via microbially or abiotically mediated processes (41). Sulfur cycling is also important within ancient hydrothermal systems, deep terrestrial aquifers, and in applied fields such as nuclear waste disposal. The reaction kinetics of  $\text{SO}_4^{2-}$  reduction by  $\text{H}_2$  have been investigated in a two-phase (water plus gas) experiment conducted under hydrothermal conditions (42). Several conditions that enhance reduction kinetics were identified, including temperature, the pH-dependent speciation of  $\text{SO}_4^{2-}$ , and the initial presence of  $\text{H}_2\text{S}$  to contribute to the formation of  $\text{S}_2\text{O}_3^{2-}$  and  $\text{S}_x^{2-}$  intermediates. Our results suggest that conditions in the Piccard mixing zone, where fluid residence times are estimated to be on the order of hours to days, support the reduction of  $\text{SO}_4^{2-}$  to intermediate oxidation state sulfur species such as elemental S,  $\text{S}_2\text{O}_3^{2-}$ , and  $\text{S}_x^{2-}$ .

The existence of a chemosynthetic subsurface biosphere inhabiting fractures in the shallow oceanic crust has been widely discussed (43). Evidence for subsurface life at oceanic spreading centers ranges from direct observations of microbial blooms

following eruptive events (44), to microbial communities inhabiting the surface and interior of young basaltic crust (45), to indirect measurements of chemical signatures in venting fluids that are presumed to be generated by thermal degradation of sub-seafloor microbial biomass (46). For example, elevations in long-chained and cyclic hydrocarbons and microbial lipid residues have been identified in high- and low-temperature vents, relative to their abundances in seawater (46). Some endmember fluids, including those at Piccard and Von Damm vent fields along the Mid-Cayman Rise, contain lower bulk DOC concentrations than ambient seawater, implying that thermal degradation at high temperatures is an important DOC removal mechanism in deep-sea vents (47, 48). In contrast, lower temperature vent fluids contain elevated DOC and microbial cell counts that are higher than ambient seawater (6, 47, 49).

Past studies have documented substantial depletions in  $H_2$  and enrichments in  $CH_4$  in low-temperature mixed hydrothermal vent fluids relative to values expected for conservative mixing (14, 15, 21, 22). Due to the presence of active microbial ecosystems in contact with the fluids (16, 17) and measured temperatures below 122 °C, the  $H_2$  depletions and  $CH_4$  enrichments in those studies were attributed to active microbial methanogenesis. Here, we demonstrate that  $H_2$  depletions and  $CH_4$  enrichments may, instead, reflect abiotic and thermogenic reaction pathways such as those occurring within hydrothermal mixing zones at the Piccard vent field at temperatures in excess of the known limits to life.

In general, previous studies that estimate Gibbs free energy available to support the subsurface biosphere in hydrothermal settings do not consider abiotic and thermogenic reactions that consume  $H_2$  and generate  $CH_4$  and  $C_{2-4}$  alkanes. To further quantify the implications of abiotic reactions on the energy landscape for the subsurface biosphere at Piccard, two geochemical mixing models were constructed that allow calculation of the maximum amount of potential chemical energy available to support five chemolithoautotrophic metabolic pathways using an approach that is similar to previous investigations (7, 50) (see Fig. 3 for metabolic reactions; see *SI Appendix* for calculation details). Both models involved incremental mixing of a hydrothermal fluid with 2 °C seawater over a temperature range of 160 to 5 °C at 500-bar pressure. For the first model, the starting composition of the hydrothermal fluid represents a conservative mixture of the endmember Beebe Vent fluid with anaerobic seawater to achieve a Mg concentration identical to the Hot Chimlet 1 fluid (*SI Appendix, Table S7*). For the second model, the composition of the fluid in 2012 (J2-619-IGT6, Table 1) was used for the starting composition of the hydrothermal fluid. At each step in the models, the potential Gibbs free energy available to support sulfate reduction, methanogenesis, methanotrophy, sulfide oxidation, and hydrogen oxidation was calculated using the calculated equilibrium distribution of aqueous species at temperatures less than or equal to 122 °C. Results demonstrate that the amount of Gibbs

free energy available for aerobic methanotrophy by  $O_2$  and sulfide oxidation by  $O_2$  increase only marginally, up to 0.1% and 0.2% per kg of mixed fluid, respectively, at a given temperature (Fig. 4 *A* and *B*). On a percent basis, a negligible amount of additional energy is made available to chemo-heterotrophic organisms that oxidize  $CH_4$ . In contrast, the potential chemical energy available for both methanogenesis involving reduction of  $CO_2$  by  $H_2$  and for hydrogenotrophic  $SO_4^{2-}$  reduction is reduced by 71 to 86% across the habitable temperature range (Fig. 4 *C* and *D*). In addition, the potential energy available for  $H_2$  oxidation by  $O_2$  is reduced by 1 to 84%, with the greatest impact at 10 °C (Fig. 4*E*). Within 50 to 90 °C mixing regimes where  $H_2$ -utilizing metabolic reactions may otherwise be expected to dominate, the energy landscape shifts to favor  $O_2$ -utilizing reactions. While thermogenic degradation of biomass can release energy to support chemo-heterotrophic organisms in submarine hydrothermal systems, our study demonstrates that abiotic processes may substantially reduce the amounts of  $H_2$ -based energy available to the subsurface biosphere on Earth. This abiotic  $H_2$  sink could vastly affect global  $H_2$  budgets and should be considered in tandem with biologically mediated sinks in global  $H_2$  mass balance models.

## Materials and Methods

**Hydrothermal Vent Fluid Sampling.** Hydrothermal fluid samples were collected by ROV *Jason II* during cruise AT18-16 aboard the RV *Atlantis* in January 2012 and by HROV *Nereus* during cruise FK008 aboard the RV *Falkor* in June 2013, following the approach reported in McDermott et al. (25). All fluids were collected using titanium isobaric gas-tight (IGT) samplers (51). Replicate samples were collected at each orifice when feasible. Fluid temperatures were monitored continuously with thermocouples mounted flush to the inlet of each IGT during the ~2 min required to fill each sampler. A National Institute of Standards and Technology temperature calibrator was used to confirm that all thermocouples were accurate to  $\pm 2$  °C. Reported temperatures for each sample (Table 1) reflect the maximum measured temperature recorded during its collection. The elapsed time interval between sampling on the seafloor and sample recovery and processing ranged from 5 to 20 h due to differences in dive duration. Onboard extraction and processing of vent fluid samples took place within 24 h of sampler recovery.

**Analytical Methods.** Shipboard sampling handling and analysis, as well as shore-based analysis, were performed for pH, volatile species, nonvolatile species, and C, S, and Sr isotopes as in McDermott et al. (25). Measured metal concentrations in the dissolved, filter, and dregs fractions are reported in *SI Appendix, Tables S4–S6*. Concentration units for species measured at sea, including  $H_2$ ,  $CH_4$ , and  $\Sigma H_2S$ , were converted from moles per liter solution to moles per kilogram solution using a uniform fluid density of 1.025 kg/L. The analytical uncertainty (2s) was  $\pm 0.05$  units for pH (25 °C, 1 atm),  $\pm 5\%$  for dissolved  $\Sigma CO_2$ ,  $CH_4$ ,  $C_2H_6$ ,  $C_3H_8$ ,  $\Sigma NH_4$ , and  $H_2$  and  $\pm 10\%$  for dissolved  $n-C_4H_{10}$ ,  $i-C_4H_{10}$ , and  $\Sigma H_2S$ . Analytical uncertainties (2s) were  $\pm 3\%$  for dissolved Na, Cl, Ca, K,  $SO_4$ , Mg,  $SiO_2$ , and Sr;  $\pm 5\%$  for dissolved Li, Rb, Fe, Mn, Zn, Cu, Al, Pb, Co, and Cd; and  $\pm 10\%$  for dissolved Br and Ag. The pooled SD (2s) for replicate samples was  $\pm 0.3\%$  for  $\delta^{13}C_{CO_2}$  and  $\pm 0.8\%$  for  $\delta^{13}C_{CH_4}$  and the instrumental analytical uncertainty (2s) was  $\pm 0.4\%$  for  $\delta^{13}C_{C_2H_6}$ ,  $\pm 0.7\%$  for  $\delta^{13}C_{C_3H_8}$ , and  $\pm 0.3\%$  for  $\delta^{34}S_{\Sigma H_2S}$ .

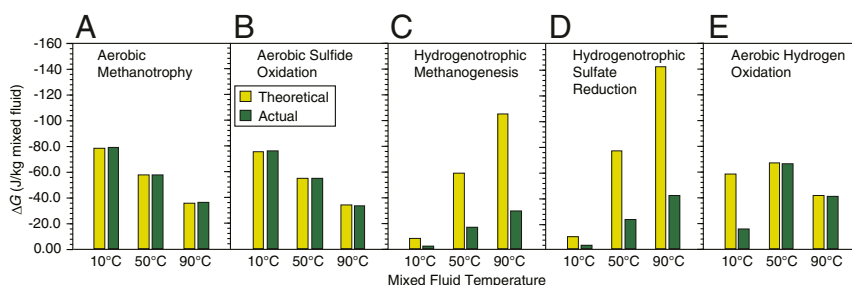


**Fig. 4.** Catabolic energy available (joules per kilogram mixed fluid) to support five microbial metabolic pathways (A–E) in 10, 50, and 90 °C Piccard mixing zone fluids. Greater energy availability is indicated by more negative  $\Delta G$  values. Energy was determined for a theoretical mixed fluid reflecting conservative endmember–seawater mixing (yellow bars) and for the actual measured mixed fluid composition that is affected by abiotic and thermogenic processes (green bars).

**Mixed and Endmember Fluid Compositions.** At high temperatures (>300 °C) and low water/rock ratio, hydrothermal fluids undergo near quantitative removal of  $Mg^{2+}$  and  $SO_4^{2-}$  during fluid–rock reaction with basalt and gabbro (52–55). The measurable dissolved  $Mg^{2+}$  in high-temperature ridge-crest hydrothermal fluids can be attributed to the dead volume of the IGT samplers (~4 mL), which are prefilled with bottom seawater prior to deployment, and to inadvertent entrainment of ambient seawater during sample collection. The composition of the zero- $Mg^{2+}$  endmembers prior to mixing were calculated via least-squares regression of an individual conservative chemical species as a function of  $Mg^{2+}$  for all samples from one vent orifice, weighted to pass through the background seawater composition and extrapolated to 0 mmol/kg  $Mg^{2+}$ .

Diffuse hydrothermal fluids (45 to 149 °C) are produced when a zero- $Mg^{2+}$  “endmember” fluid mixes with ambient seawater below the seafloor and/or within chimney structures prior to sampling. Diffuse fluid compositions therefore reflect two-component mixing of these two compositionally distinct fluids. Nonconservative behavior occurs during subsurface mixing for some species reported here (e.g.,  $Ca^{2+}$ ,  $Sr^{2+}$ ,  $SO_4^{2-}$ ,  $\Sigma NH_4$ ,  $\Sigma HCOOH$ ,  $H_2$ ,  $\Sigma H_2S$ ,  $CH_4$ ,  $C_2+$  alkanes, and transition metals). Only measured abundances are reported for these nonconservative species in lower temperature mixed fluids (Tables 1 and 2 and *SI Appendix, Tables S1 and S2*), because extrapolation to an end-member composition has no physical meaning in these instances.

**Thermodynamic Affinity Calculations.** The affinity for the reduction of  $CO_2$  with  $H_2$  to produce  $HCOO^-$  and  $H^+$  via reaction 1 was calculated as in McDermott et al. (29).

**Numerical Geochemical Mixing Model.** See *SI Appendix*.

**Data Availability.** All study data are included in the article and *SI Appendix*.

**ACKNOWLEDGMENTS.** Financial support was provided by the National Aeronautics and Space Administration (NASA) Astrobiology program (Awards NNX09AB75G and 80NSSC19K1427 to C.R.G. and J.S.S.) and the NSF (Award OCE-1061863 to C.R.G. and J.S.S.). Ship and vehicle time for cruise FK008 was provided by the Schmidt Ocean Institute. We thank the ROV *Jason II* and HROV *Nereus* groups, and the captain, officers, and crew of R/V *Atlantis* (AT18-16) and R/V *Falkor* (FK008) for their dedication to skillful operations at sea. We thank our scientific colleagues from both cruises, as well as Meg Tivey, Frieder Klein, and Scott Wankel for insightful discussions. We are grateful to the editor and two anonymous reviewers for providing helpful comments and suggestions.

1. H. Staudigel, S. R. Hart, Alteration of basaltic glass: Mechanisms and significance for the oceanic crust-seawater budget. *Geochim. Cosmochim. Acta* **47**, 337–350 (1983).
2. C. R. German, W. E. Seyfried Jr., “Hydrothermal processes” in *Treatise on Geochemistry: Second Edition*, H. D. Holland, K. K. Turekian, Eds. (Elsevier, 2014), Vol. 8, pp. 191–233.
3. A. D. Opatkiewicz, D. A. Butterfield, J. A. Baross, Individual hydrothermal vents at Axial Seamount harbor distinct seafloor microbial communities. *FEMS Microbiol. Ecol.* **70**, 413–424 (2009).
4. M. Perner et al., Driving forces behind the biotope structures in two low-temperature hydrothermal venting sites on the southern Mid-Atlantic Ridge. *Environ. Microbiol. Rep.* **3**, 727–737 (2011).
5. K. Nakamura, K. Takai, Theoretical constraints of physical and chemical properties of hydrothermal fluids on variations in chemolithotrophic microbial communities in seafloor hydrothermal systems. *Prog. Earth Planet. Sci.* **1**, 1–24 (2014).
6. J. Reveillaud et al., Seafloor microbial communities in hydrogen-rich vent fluids from hydrothermal systems along the Mid-Cayman Rise. *Environ. Microbiol.* **18**, 1970–1987 (2016).
7. T. M. McCollom, E. L. Shock, Geochemical constraints on chemolithoautotrophic metabolism by microorganisms in seafloor hydrothermal systems. *Geochim. Cosmochim. Acta* **61**, 4375–4391 (1997).
8. S. Sievert, C. Vetriani, Chemoautotrophy at deep-sea vents: Past, present, and future. *Oceanography* **25**, 218–233 (2012).
9. A.-L. Reysenbach, E. Shock, Merging genomes with geochemistry in hydrothermal ecosystems. *Science* **296**, 1077–1082 (2002).
10. R. E. Anderson et al., Genomic variation in microbial populations inhabiting the marine seafloor at deep-sea hydrothermal vents. *Nat. Commun.* **8**, 1114 (2017).
11. J. P. Amend, T. M. McCollom, M. Hentscher, W. Bach, Catabolic and anabolic energy for chemolithoautotrophs in deep-sea hydrothermal systems hosted in different rock types. *Geochim. Cosmochim. Acta* **75**, 5736–5748 (2011).
12. M. Hentscher, W. Bach, Geochemically induced shifts in catabolic energy yields explain past ecological changes of diffuse vents in the East Pacific Rise 9°50'N area. *Geochem. Trans.* **13**, 2 (2012).
13. H. Dahle, I. Økland, I. H. Thorseth, R. B. Pederesen, I. H. Steen, Energy landscapes shape microbial communities in hydrothermal systems on the Arctic Mid-Ocean Ridge. *ISME J.* **9**, 1593–1606 (2015).
14. K. L. Von Damm, M. D. Lilley, “Diffuse flow hydrothermal fluids from 9° 50' N East Pacific Rise: Origin, evolution and biogeochemical controls” in *The Subseafloor Biosphere at Mid-Ocean Ridges*, W. S. D. Wilcock, E. F. Delong, D. S. Kelley, J. A. Baross, S. C. Cary, Eds. (American Geophysical Union, 2004), Vol. 144, pp. 245–268.
15. S. D. Wankel et al., Influence of subsurface biosphere on geochemical fluxes from diffuse hydrothermal fluids. *Nat. Geosci.* **4**, 461–468 (2011).
16. J. McNichol et al., Primary productivity below the seafloor at deep-sea hot springs. *Proc. Natl. Acad. Sci. U.S.A.* **115**, 6756–6761 (2018).
17. J. McNichol et al., Assessing microbial processes in deep-sea hydrothermal systems by incubation at in situ temperature and pressure. *Deep. Res. Part I Oceanogr. Res. Pap.* **115**, 221–232 (2016).
18. A. Gartman et al., Sulfide oxidation across diffuse flow zones of hydrothermal vents. *Aquat. Geochem.* **17**, 583–601 (2011).
19. C. S. Fortunato, B. Larson, D. A. Butterfield, J. A. Huber, Spatially distinct, temporally stable microbial populations mediate biogeochemical cycling at and below the seafloor in hydrothermal vent fluids. *Environ. Microbiol.* **20**, 769–784 (2018).
20. J. B. Sylvan et al., Evidence for microbial mediation of seafloor nitrogen redox processes at Loihi Seamount, Hawaii. *Geochim. Cosmochim. Acta* **198**, 131–150 (2017).
21. D. A. Butterfield et al., “Mixing, reaction and microbial activity in the sub-seafloor revealed by temporal and spatial variation in diffuse flow vents at Axial volcano” in *The Subseafloor Biosphere at Mid-Ocean Ridges*, W. S. D. Wilcock, E. F. Delong, D. S. Kelley, J. A. Baross, S. C. Cary, Eds. (American Geophysical Union, 2004), Vol. 144, pp. 269–289.
22. G. Proskurowski, M. D. Lilley, E. J. Olson, Stable isotopic evidence in support of active microbial methane cycling in low-temperature diffuse flow vents at 9°50'N East Pacific Rise. *Geochim. Cosmochim. Acta* **72**, 2005–2023 (2008).
23. R. A. Beinart, A. Gartman, J. G. Sanders, G. W. Luther, P. R. Girguis, The uptake and excretion of partially oxidized sulfur expands the repertoire of energy resources metabolized by hydrothermal vent symbioses. *Proc. Biol. Sci.* **282**, 20142811 (2015).
24. J. C. Kinsey, C. R. German, Sustained volcanically-hosted venting at ultraslow ridges: Piccard hydrothermal field, Mid-Cayman Rise. *Earth Planet. Sci. Lett.* **380**, 162–168 (2013).
25. J. M. McDermott, S. P. Sylva, S. Ono, C. R. German, S. Seewald, Geochemistry of fluids from Earth's deepest ridge-crest hot-springs: Piccard hydrothermal field, Mid-Cayman Rise. *Geochim. Cosmochim. Acta* **228**, 95–118 (2018).
26. S. L. Worman, L. F. Pratson, J. A. Karson, W. H. Schlesinger, Abiotic hydrogen ( $H_2$ ) sources and sinks near the Mid-Ocean Ridge (MOR) with implications for the seafloor biosphere. *Proc. Natl. Acad. Sci. U.S.A.* **117**, 13283–13293 (2020).
27. J. H. Trefry et al., Trace metals in hydrothermal solution from Cleft segment on the southern Juan de Fuca Ridge. *J. Geophys. Res.* **99**, 4925–4935 (1994).
28. K. Takai et al., Geochemical and microbiological evidence for a hydrogen-based, hyperthermophilic subsurface lithoautotrophic microbial ecosystem (HyperSLiME) beneath an active deep-sea hydrothermal field. *Extremophiles* **8**, 269–282 (2004).
29. J. M. McDermott, J. S. Seewald, C. R. German, S. P. Sylva, Pathways for abiotic organic synthesis at submarine hydrothermal fields. *Proc. Natl. Acad. Sci. U.S.A.* **112**, 7668–7672 (2015).
30. S. Q. Lang et al., Deeply-sourced formate fuels sulfate reducers but not methanogens at Lost City hydrothermal field. *Sci. Rep.* **8**, 755 (2018).
31. T. M. Joyce, A. Hernandez-Guerra, M. Smethie Jr., Zonal circulation in the NW Atlantic and Caribbean from a meridional World Ocean Circulation Experiment hydrographic section at 66°W. *J. Geophys. Res.* **106**, 22095–22113 (2001).
32. D. L. Eldridge, W. Guo, J. Farquhar, Theoretical estimates of equilibrium sulfur isotope effects in aqueous sulfur systems: Highlighting the role of isomers in the sulfite and sulfoxylate systems. *Geochim. Cosmochim. Acta* **195**, 171–200 (2016).
33. G. W. Luther III et al., Chemical speciation drives hydrothermal vent ecology. *Nature* **410**, 813–817 (2001).
34. K. M. Mullaugh et al., Voltammetric (micro)electrodes for the in situ study of  $Fe^{2+}$  oxidation kinetics in hot springs and  $S_2O_3^{2-}$  production at hydrothermal vents. *Electroanalysis* **20**, 280–290 (2008).
35. I. M. Head, D. M. Jones, S. R. Larter, Biological activity in the deep subsurface and the origin of heavy oil. *Nature* **426**, 344–352 (2003).
36. M. Schoell, Multiple origins of methane in the Earth. *Chem. Geol.* **71**, 1–10 (1988).
37. M. Schoell, The hydrogen and carbon isotopic composition of methane from natural gases of various origins. *Geochim. Cosmochim. Acta* **44**, 649–661 (1980).
38. F. Lorant, A. Prinzhofer, F. Behar, A. Y. Huc, Carbon isotopic and molecular constraints on the formation and the expulsion of thermogenic hydrocarbon gases. *Chem. Geol.* **147**, 249–264 (1998).
39. M. A. Rooney, G. E. Claypool, H. M. Chung, Modeling thermogenic gas generation using a carbon isotope ratios of natural gas hydrocarbons. *Chem. Geol.* **126**, 219–232 (1995).
40. E. P. Reeves, J. M. McDermott, J. S. Seewald, The origin of methanethiol in midocean ridge hydrothermal fluids. *Proc. Natl. Acad. Sci. U.S.A.* **111**, 5474–5479 (2014).
41. H. G. Machel, Bacterial and thermochemical sulfate reduction in diagenetic settings—old and new insights. *Sediment. Geol.* **140**, 143–175 (2001).
42. L. Truche et al., Experimental reduction of aqueous sulphate by hydrogen under hydrothermal conditions: Implication for the nuclear waste storage. *Geochim. Cosmochim. Acta* **73**, 4824–4835 (2009).

43. B. N. Orcutt, J. B. Sylvan, N. J. Knab, K. J. Edwards, Microbial ecology of the dark ocean above, at, and below the seafloor. *Microbiol. Mol. Biol. Rev.* **75**, 361–422 (2011).
44. J. L. Meyer, N. H. Akerman, G. Proskurowski, J. A. Huber, Microbiological characterization of post-eruption “snowblower” vents at Axial Seamount, Juan de Fuca Ridge. *Front. Microbiol.* **4**, 153 (2013).
45. C. M. Santelli *et al.*, Abundance and diversity of microbial life in ocean crust. *Nature* **453**, 653–656 (2008).
46. M. Brault, B. R. T. Simoneit, J. C. Marty, A. Saliot, Hydrocarbons in waters and particulate material from hydrothermal environments at the East Pacific Rise, 13°N. *Org. Geochem.* **12**, 209–219 (1988).
47. S. Q. Lang, D. A. Butterfield, M. D. Lilley, H. P. Johnson, J. I. Hedges, Dissolved organic carbon in ridge-axis and ridge-flank hydrothermal systems. *Geochim. Cosmochim. Acta* **70**, 3830–3842 (2006).
48. J. A. Hawkes *et al.*, Efficient removal of recalcitrant deep-ocean dissolved organic matter during hydrothermal circulation. *Nat. Geosci.* **8**, 856–860 (2015).
49. S. Q. Lang, D. A. Butterfield, M. Schulte, D. S. Kelley, M. D. Lilley, Elevated concentrations of formate, acetate and dissolved organic carbon found at the Lost City hydrothermal field. *Geochim. Cosmochim. Acta* **74**, 941–952 (2010).
50. T. M. McCollom, Geochemical constraints on sources of metabolic energy for chemolithoautotrophy in ultramafic-hosted deep-sea hydrothermal systems. *Astrobiology* **7**, 933–950 (2007).
51. J. S. Seewald, K. W. Doherty, T. R. Hammar, S. P. Liberatore, A new gas-tight isobaric sampler for hydrothermal fluids. *Deep. Res. Part I Oceanogr. Res. Pap.* **49**, 189–196 (2002).
52. J. L. Bischoff, F. W. Dickson, Seawater-basalt interaction at 200°C and 500 bars: Implications for origin of seafloor heavy-metal deposits and regulation of seawater chemistry. *Earth Planet. Sci. Lett.* **25**, 385–397 (1975).
53. M. J. Mottl, H. D. Holland, Chemical exchange during hydrothermal alteration of basalt by seawater—I. Experimental results for major and minor components of seawater. *Geochim. Cosmochim. Acta* **42**, 1103–1115 (1978).
54. W. E. Seyfried, J. L. Bischoff, Experimental seawater-basalt interaction at 300°C, 500 bars, chemical exchange, secondary mineral formation and implications for the transport of heavy metals. *Geochim. Cosmochim. Acta* **45**, 135–147 (1981).
55. K. L. Von Damm *et al.*, Chemistry of submarine hydrothermal solutions at 21°N, East Pacific Rise. *Geochim. Cosmochim. Acta* **49**, 2197–2220 (1985).
56. J. W. Johnson, E. H. Oelkers, H. C. Helgeson, SUPCRT92: A software package for calculating the standard molal thermodynamic properties of minerals, gases, aqueous species, and reactions from 1 to 5000 bar and 0 to 1000°C. *Comput. Geosci.* **18**, 899–947 (1992).
57. P. Toulmin, P. B. Barton, A thermodynamic study of pyrite and pyrrhotite. *Geochim. Cosmochim. Acta* **28**, 641–671 (1964).